that Se_{10}^{2+} may not retain this structure in solution. There is a considerable difference between the solution and solid-state electronic spectra of the Se_{10}^{2+} cation,[2] and ^{77}Se NMR studies have provided evidence for intramolecular exchange and isomerization in both SO_2 and 100% H_2SO_4 solution.[27] In contrast, the ^{77}Se NMR spectrum of $Te_2Se_8^{2+}$ in 100% H_2SO_4 shows no sign of exchange and is consistent with the solid-state structure.[28] The $Te_2Se_6^{2+}$ and Se_8^{2+} cations also retain their unique solid-state structures in solution.[27,29]

Acknowledgment. We thank the Natural Sciences and Engineering Research Council of Canada for financial support.

Registry No. **1a**, 58249-21-1; **1b**, 107453-36-1; **2**, 107556-03-6; **3**, 107453-35-0; Te, 13494-80-9; Se, 7782-49-2; AsF_5, 7784-36-3; SO_2, 7446-09-5; SbF_5, 7783-70-2; S, 7704-34-9.

Supplementary Material Available: Tables VI and VII, containing bond distances and bond angles in the anions and final anisotropic thermal parameters, respectively (7 pages); Table VIII, containing final structure factor amplitudes (43 pages). Ordering information is given on any current masthead page.

(27) Burns, R. C.; Collins, M. J.; Gillespie, R. J.; Schrobilgen, G. J.; *Inorg. Chem.* **1986**, *25*, 4465.
(28) Collins, M. J. Ph.D. Thesis, McMaster University, 1984.
(29) Collins, M. J.; Gillespie, R. J. *Inorg. Chem.* **1984**, *23*, 1975.

Contribution from the Institute of Molecular Physics of the Polish Academy of Sciences, 60-179 Poznań, Poland, and the Faculty of Chemistry, Jagiellonian University, 30-060 Kraków, Poland

Crystal Structure and Magnetic and EPR Studies of Bis[cinchoninium tetrachlorocuprate(II)] Trihydrate Single Crystals with a Weak Exchange Coupling

K. Dyrek,[2] J. Goslar,[1] S. A. Hodorowicz,[2] S. K. Hoffmann,*[1] B. J. Oleksyn,[2] and A. Wesełucha-Birczyńska[3]

Received April 25, 1986

The crystal structure of bis[cinchoninium tetrachlorocuprate(II)] trihydrate, $[(C_{19}H_{24}N_2O)CuCl_4]_2 \cdot 3H_2O$, has been established by single-crystal X-ray diffraction methods. The crystals are orthorhombic, space group $P2_12_12_1$, with unit cell parameters a = 15.414 (3), b = 36.719 (6), and c = 7.974 (2) Å for Z = 4. The asymmetric unit consists of two tetrahedral $CuCl_4^{2-}$ anions, which are linked to two doubly protonated cinchonine molecules and three water molecules by hydrogen bonds. The $CuCl_4^{2-}$ tetrahedrons are approximately D_{2d} flattened with the average Cl–Cu–Cl angle along the flattening axes being 145° and the ⟨Cu–Cl⟩ distance being 2.25 Å. The magnetic susceptibility obeys the Curie law in the temperature range from 4.2 to 350 K, and the crystal can be treated as magnetically diluted. The exchange coupling between magnetically nonequivalent Cu(II) ions, determined from a computer analysis of two-component EPR spectra, is $|J|$ = 0.0030 (5) cm^{-1} at 298 K and increases at low temperatures. Reflectance UV–vis spectra contain d–d bands, $xy \rightarrow (xz,yz)$ = 9100 cm^{-1} and $xy \rightarrow z^2$ = 11 100 cm^{-1}, and charge-transfer bands at 22 500 and 26 000 cm^{-1}. The band positions are analyzed in terms of ligand field theory, by addition to the crystal field electrostatic terms of the destabilization terms from covalency of the Cu–Cl bonds described by the angular overlap model. The EPR parameters, $g_\parallel$ = 2.292 (4) and $g_\perp$ = 2.051 (4), are discussed in terms of the MO theory, including charge-transfer, orbital overlap, and ligand spin–orbit-coupling contributions.

Introduction

Cinchonine (cin = $C_{19}H_{22}N_2O$) belongs to the group of the four most important alkaloids of the *Cinchona* tree bark. Like the other members of this group, it is a biologically active compound and has an antimalarial activity comparable to that of quinine.[4] The conformation of quinine molecule has been recently described for its derivative 10-hydroxy-10-methyl-10,11-dihydroquinine,[5] while the absolute configuration of cinchonine (Figure 1) was determined in the course of the X-ray structure analysis of cinchoninium tetrachlorocadmate(II) dihydrate,[6] which is one of the isomorphous compounds of the general formula $cin \cdot 2HCl \cdot MCl_2 \cdot 2H_2O$ (M = Cd, Co, Zn, Hg).[6,7] Their crystalline structure consists of M ions tetrahedrally surrounded by chlorine anions that form a system of hydrogen bonds with nitrogen atoms of $(cinH_2)^{2+}$ cations and with water molecules. This can be interpreted as a weak indirect interaction of M with cinchonine, as suggested by IR data.[7] The MCl_4^{2-} complexes are well separated one from another in the crystal. Thus no magnetic or superexchange couplings between Co(II) ions were detected by EPR[8] and magnetic susceptibility[9] in $(cinH_2)(CoCl_4) \cdot 2H_2O$.

The fact that the compound with M = Cu is not isomorphous with the above series prompted us to perform X-ray diffraction, magnetic, EPR, and UV–vis studies on this compound as well as a detailed analysis of the electronic structure of $CuCl_4^{2-}$ complexes in the crystalline state.

Experimental Section

Preparation of the Compound. Bis[cinchoninium tetrachlorocuprate(II)] trihydrate was prepared according to Dyrek's method.[7] A solution of 10 mg of cinchonine (Koch-Light) in 60 mL of HCl (1:1) was mixed with 50 mL of $CuCl_2$ (0.5 M). The color of the solution changed rapidly from blue to green. The solution was heated for about 0.5 h on a water bath. After the solution was allowed to stand and cool, well-shaped greenish yellow crystals deposited. The crystals were filtered, washed with ethanol, and dried in the air. The crystals with a prismatic habit were elongated along the c-axis with well-developed (010) faces.

Crystal Structure Determination. The lattice parameters, determined together with other crystal data,[10] were confirmed and refined in the autoindexing procedure from the setting angles of 15 reflections. The intensities of reflections were measured with a four-circle automatic CAD-4 Enraf Nonius diffractometer. The crystal and data collection

(1) Institute of Molecular Physics of the Polish Academy of Sciences.
(2) Jagiellonian University.
(3) Regional Laboratory of Physico-Chemical Analyses and Structural Research, Jagiellonian University, 30-060 Kraków, Poland.
(4) Cheng, C. C. *J. Pharm. Sci.* **1971**, *60*, 1596–1598.
(5) Suszko-Purzycka, A.; Lipińska, T.; Piotrowska, E.; Oleksyn, B. J. *Acta Crystallogr., Sect. C: Cryst. Struct. Commun.* **1985**, *C41*, 977–980.
(6) Oleksyn, B. J.; Stadnicka, K. M.; Hodorowicz, S. A. *Acta Crystallogr., Sect. B: Struct. Crystallogr. Cryst. Chem.* **1978**, *B34*, 811–816.
(7) Dyrek, M. *Rocz. Chem.* **1976**, *50*, 2027–2034.
(8) Drulis, H.; Dyrek, K.; Hoffmann, K. P.; Hoffmann, S. K.; Wesełucha-Birczyńska, A. *Inorg. Chem.* **1985**, *24*, 4009–4012.
(9) Dyrek, K.; Dyrek, M.; Wesełucha-Birczyńska, A. *Polyhedron* **1985**, *4*, 169–172.
(10) Chojnacki, J.; Oleksyn, B. J.; Hodorowicz, S. A. *Rocz. Chem.* **1975**, *49*, 429–431.

0020-1669/87/1326-1481$01.50/0

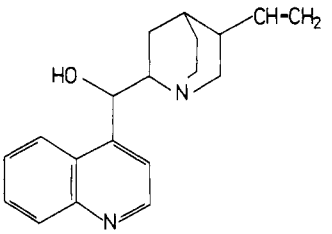

Figure 1. Structural formula of the cinchonine molecule.

Table I. Crystal and Data Collection Parameters for $[(C_{19}H_{24}N_2O)^{2+}(CuCl_4)^{2-}]_2 \cdot 3H_2O$

formula (M_r)	$[(C_{19}H_{24}N_2O)^{2+}(CuCl_4)^{2-}]_2 \cdot 3H_2O$ (1057.58)
a, Å	15.414 (3)
b, Å	36.719 (6)
c, Å	7.974 (2)
V, Å^3	4513 (2)
cryst syst	orthorhombic
Z	4
ρ(exptl), g cm^{-3}	1.57 (1)
ρ(calcd), g cm^{-3}	1.56
space group	$P2_12_12_1$
cryst dimens, mm	0.3 × 0.2 × 0.2
radiation	Cu Kα (λ = 1.5418 Å)
temp, °C	20
monochromator	graphite
abs coeff, μ(Cu Kα), cm^{-1}	57.3 (no cor made)
scan mode	ω–2θ
scan range, deg	0.6 + 0.3 tan θ
2θ limits, deg	1.0–72.0
reflcns collcd	$+h,+k,+l$
stds monitored	2 stds every 46 reflcns
no. of reflcns collcd	5196
no. of unique reflcns	4426
no. of reflcns with $\|F_o\| \geq 3\ \sigma(F_o)$	3335
no. of params varied	514
w^{-1}	$\sigma^2(F_o) + (gF_o)^2$, g = 0.0031
$R(F) = \sum\|\|F_o\| - \|F_c\|\|/\sum\|F_o\|$	0.078
$R_w(F) = [\sum w(\|F_o\| - \|F_c\|)^2/\sum w\|F_o\|^2]^{1/2}$	0.081
largest peaks on final diff map, e Å^{-3}	0.75,[a] 0.65,[b] 0.59[c]

[a] x/a = 0.5421, y/b = 0.2462, z/c = 0.7686. [b] x/a = 0.5362, y/b = 0.3005, z/c = 0.7432. [c] x/a = 0.0967, y/b = −0.0540, z/c = 1.1994.

parameters are given in Table I. The data were corrected for Lorentz and polarization effects but not for absorption. The calculations were carried out on a CYBER 72 computer using the SHELX76 system of programs.[11] Scattering factors for Cl, O, N, C, and H were those used by the program, while the factors for Cu were taken from ref 12 and 13. The structure was solved by the heavy-atom method. When the positions of all non-hydrogen atoms, with the exception of O(W3), were determined in the series of subsequent difference Fourier maps (R = 0.17), several cycles of anisotropic least-squares refinements of Cu and Cl atoms and isotropic refinement of the others gave R = 0.13. O(W3) was then revealed and introduced to the further refinement procedure in which the structure was divided into segments because of the limited number of parameters that could be refined simultaneously. In the last cycles of the anisotropic refinement of all the atoms, the positions of 38 hydrogen atoms were calculated and found in the difference Fourier maps, but they were not refined. At this stage (R = 0.078) the refinement for the copper–chlorine complexes together with water oxygens was considered as completed since the shifts of atomic coordinates were less than 0.02 of their estimated standard deviations. Tables II and III list the atomic coordinates and selected interatomic distances and angles, respectively. Listings of hydrogen atom positions, h, k, l, F_o, F_c, and thermal parameters are available as supplementary material.

Physical Measurements. Magnetic susceptibility data were collected in the temperature range 4.2–350 K on powdered samples by using a Faraday balance at 0.8 T. The data were corrected for the diamagnetism of constituent atoms (χ_{dia} = −334×10^{-6} emu).

EPR spectra of powdered samples and single crystals were recorded on a RADIOPAN SE/X-2543 spectrometer with a TE_{102} rectangular cavity and 100-kHz modulation. The magnetic field was monitored with an automatically tracking RADIOPAN JTM-41 NMR gaussmeter, and DPPH was used as an internal frequency standard. The single-crystal angular dependence of the EPR spectra was recorded in the crystallographic axes system a, b, c at 5° intervals. Because of a relatively low resolution of the two-component EPR spectra, the parameters of the individual lines were determined by computer simulation.

Reflectance UV–vis spectra were recorded on a Beckman DK 2A spectrometer in the range of 200–2500 nm with a $BaSO_4$ as a standard.

Table II. Fractional Atomic Coordinates (×10^4) and Average Temperature Factors (Å^2 × 10^3)

atom	x	y	z	U(av)[a]
Cu(1)	5445 (1)	2735 (1)	7594 (2)	36
Cu(2)	182 (1)	4430 (1)	7961 (2)	41
Cl(1)	4614 (2)	2545 (1)	5453 (4)	46
Cl(2)	6241 (2)	2557 (1)	9805 (4)	47
Cl(3)	4361 (2)	2979 (1)	9137 (4)	49
Cl(4)	6562 (2)	2918 (1)	5981 (4)	46
Cl(5)	32 (3)	4376 (1)	10757 (5)	76
Cl(6)	197 (3)	4159 (1)	5469 (6)	89
Cl(7)	1630 (2)	4517 (1)	8016 (7)	89
Cl(8)	−1158 (2)	4666 (1)	7607 (5)	65
O(W1)	5334 (5)	3180 (2)	12843 (11)	51
O(W2)	1750 (8)	4478 (3)	12709 (19)	99
O(W3)	−1452 (7)	4532 (2)	13452 (13)	60
N(101)	2915 (6)	1945 (2)	10537 (14)	29
C(102)	3228 (8)	2011 (3)	8793 (19)	47
C(103)	4103 (9)	1803 (4)	8494 (17)	43
C(104)	4319 (8)	1584 (3)	10092 (18)	40
C(105)	4428 (8)	1846 (4)	11556 (20)	49
C(106)	3589 (9)	2078 (4)	11738 (20)	52
C(107)	3544 (7)	1324 (3)	10415 (21)	43
C(108)	2758 (7)	1551 (3)	10984 (17)	33
C(109)	1869 (8)	1410 (3)	10322 (17)	31
C(110)	4114 (10)	1571 (4)	6946 (21)	57
C(111)	3512 (12)	1496 (5)	5792 (20)	79
O(112)	1792 (6)	1472 (2)	8556 (11)	47
N(113)	1630 (7)	263 (2)	11138 (15)	40
C(114)	1896 (9)	385 (4)	9727 (19)	47
C(115)	1983 (8)	760 (3)	9429 (19)	42
C(116)	1799 (7)	1005 (3)	10674 (17)	30
C(117)	1543 (6)	872 (3)	12236 (17)	32
C(118)	1346 (9)	1088 (3)	13667 (15)	38
C(119)	1091 (8)	949 (4)	15152 (16)	41
C(120)	990 (10)	566 (4)	15330 (19)	56
C(121)	1185 (8)	335 (4)	14035 (20)	47
C(122)	1455 (8)	488 (3)	12464 (19)	42
N(201)	3014 (6)	3088 (2)	5649 (13)	32
C(202)	2772 (10)	3020 (4)	3771 (19)	49
C(203)	1828 (9)	3160 (4)	3453 (18)	47
C(204)	1539 (8)	3367 (3)	5014 (21)	49
C(205)	1480 (8)	3096 (3)	6491 (19)	44
C(206)	2347 (9)	2900 (4)	6676 (22)	60
C(207)	2224 (7)	3665 (3)	5448 (18)	34
C(208)	3052 (7)	3485 (3)	6051 (17)	34
C(209)	3895 (7)	3666 (3)	5564 (17)	33
C(210)	1705 (14)	3392 (6)	1877 (24)	92
C(211)	2224 (18)	3597 (6)	882 (26)	118
O(212)	4049 (6)	3643 (2)	3790 (11)	42
N(213)	3653 (7)	4806 (3)	6694 (16)	48
C(214)	3464 (9)	4680 (4)	5224 (21)	54
C(215)	3552 (8)	4315 (3)	4847 (19)	44
C(216)	3842 (7)	4074 (3)	5989 (14)	32
C(217)	4030 (6)	4205 (3)	7624 (16)	31
C(218)	4357 (9)	3987 (4)	8934 (18)	44
C(219)	4558 (10)	4138 (5)	10469 (22)	67
C(220)	4487 (11)	4517 (5)	10691 (21)	66
C(221)	4175 (10)	4743 (4)	9486 (22)	58
C(222)	3968 (8)	4590 (4)	7909 (21)	51

[a] $U_{av} = {}^1/_3(U_{11} + U_{22} + U_{33})$.

Results and Discussion

Description and Discussion of the Structure. A fragment of the unit cell projected along the c axis is shown in Figure 2, and

(11) Sheldrick, G. M. Program for Crystal Structure Determination, University of Cambridge, England, 1976.
(12) *International Tables for X-ray Crystallography*; Kynoch: Birmingham, England, 1974; Vol. IV, p 99.
(13) Cromer, D. T. *Acta Crystallogr.* **1965**, *18*, 17–23.

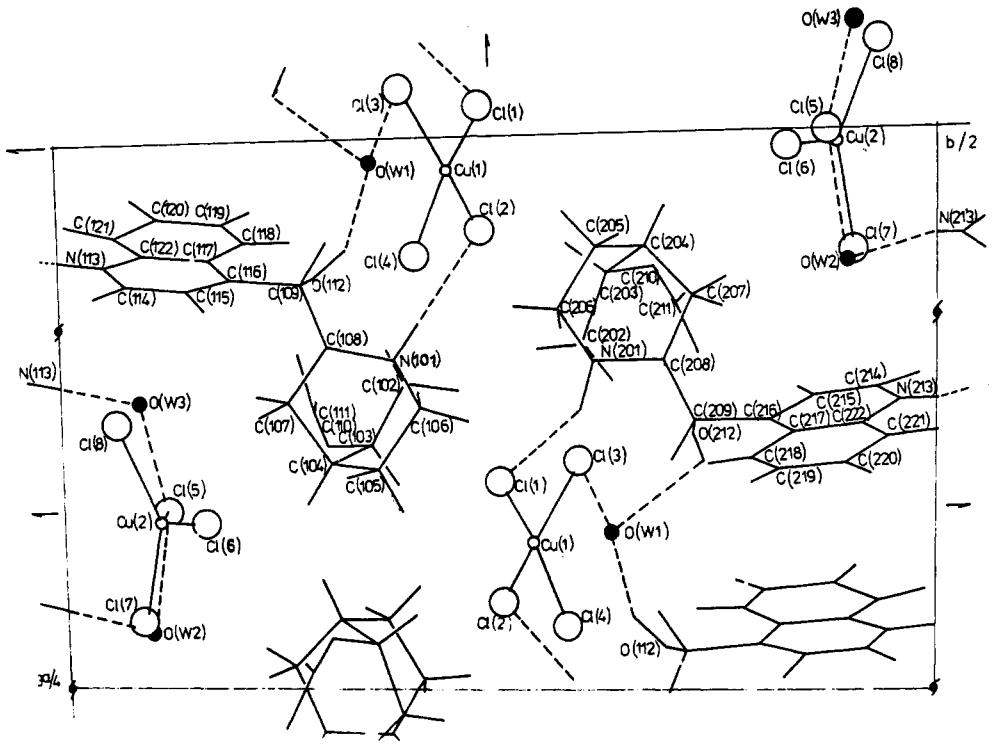

Figure 2. Fragment of the unit cell projected along $\vec{c}$.

Table III. Selected Interatomic Distances (Å) and Angles (deg)

(A) Tetrahedral Cu Complexes			
Cu(1)–Cl(1)	2.246 (4)	Cu(2)–Cl(5)	2.250 (5)
Cu(1)–Cl(2)	2.246 (4)	Cu(2)–Cl(6)	2.221 (5)
Cu(1)–Cl(3)	2.260 (4)	Cu(2)–Cl(7)	2.255 (4)
Cu(1)–Cl(4)	2.252 (4)	Cu(2)–Cl(8)	2.260 (4)
Cl(1)–Cu(1)–Cl(2)	144.9 (1)	Cl(5)–Cu(2)–Cl(6)	148.0 (2)
Cl(1)–Cu(1)–Cl(3)	96.6 (1)	Cl(5)–Cu(2)–Cl(7)	95.5 (2)
Cl(1)–Cu(1)–Cl(4)	95.4 (1)	Cl(5)–Cu(2)–Cl(8)	93.6 (2)
Cl(2)–Cu(1)–Cl(4)	96.8 (1)	Cl(6)–Cu(2)–Cl(7)	94.0 (2)
Cl(2)–Cu(1)–Cl(3)	95.3 (1)	Cl(6)–Cu(2)–Cl(8)	94.0 (2)
Cl(3)–Cu(1)–Cl(4)	139.3 (1)	Cl(7)–Cu(2)–Cl(8)	148.5 (2)

(B) Hydrogen Bonds[a]

donors (D)	acceptors (A)	D···A
O(112)	O(W1^{i})	2.75 (2)
O(212)	O(W1^{ii})	2.77 (2)
N(113^{iii})	O(W3)	2.72 (2)
N(213^{iv})	O(W2)	2.82 (2)
N(101)	Cl(2^{i})	3.17 (2)
N(201)	Cl(1)	3.18 (2)
O(W1)	Cl(3)	3.26 (2)
O(W2)	Cl(5)	3.11 (2)
O(W3)	Cl(5)	3.19 (2)
O(W3^{ii})	Cl(6)	3.31 (2)

[a] Symmetry code: (i) $x - {}^1/_2, \bar{y} + {}^1/_2, \bar{z} + 2$; (ii) $x, y, z - 1$; (iii) $\bar{x}, y + {}^1/_2, \bar{z} + {}^3/_2$; (iv) $\bar{x} + {}^1/_2, \bar{y} + 1, z + {}^1/_2$.

atomic coordinates are given in Table II. The asymmetric unit consists of the two tetrachlorocuprate anions, three water molecules and two cinchonine cations protonated at nitrogen atoms N(101), N(113) and N(201), N(213), respectively. The absolute configuration of the cinchonine molecule agrees with that in tetrachlorocadmate(II).[6] Molecules 1 and 2 differ slightly from each other in the conformation. They are engaged in the following system of hydrogen bonds: oxygen atoms of both molecules are linked to the water molecules O(W1); nitrogen atoms, N(113) and N(213), of quinoline parts form bonds with O(W3) and O(W2) respectively, while N(101) and N(201) of the quinuclidine parts are bonded to Cl(2) and Cl(1), respectively. The details of these hydrogen bonds are given in Table IIIB. The net of the hydrogen bonds leads to helicoidal packing around screw axes along the *c* direction. As a result the layers parallel to the *ac* planes

Table IV. Average Cu–Cl Distances and Flattening Angles of the Two Crystallographically Nonequivalent $CuCl_4^{2-}$ Tetrahedrons

	complex I	complex I′
$\langle R \rangle_{Cu-Cl}$, Å	2.253	2.247
β_1, deg	73.9	72.4
β_2, deg	74.3	69.7
$\langle \beta \rangle$, deg	74.1	71.1

can be observed in the structure. The contacts between the layers are of van der Waals character.

The Cu atoms are coordinated to four Cl atoms at an average distance of 2.25 Å. This value is close to those observed in various Cu complexes of similar type (see Table V). The data listed in Table III show that the differences in the Cu–Cl distances of both Cu complexes are in the range of the experimental errors (3 esd's). The bond angles, Cl–Cu–Cl, vary in the broad range 148.5 (2)–93.6 (2)°. As shown in Table III the angles Cl(1)–Cu(1)–Cl(2), Cl(3)–Cu(1)–Cl(4), and Cl(7)–Cu(2)–Cl(8), Cl(5)–Cu(2)–Cl(6) indicate a significant deviation from the ideal tetrahedral geometry for both complexes. Each of the tetrahedrons shows a flattening along one of the $\bar{4}$ axes, which leads to an approximate D_{2d} symmetry. The directions of these flattening axes are close to the *b* edge of the unit cell, as shown by the direction cosines: 0.1525, 0.9687, and –0.1961 and 0.0358, 0.9986, and –0.0382 for the Cu(1) and Cu(2) complexes, respectively. The distances between the centers of the edges of the tetrahedrons measured along the flattening axis are marked in Figure 3 as L_1, L_2, and L_3. The value of L_1 for the Cu(2) complex is about 16% lower than that for the Cu(1) complex. This fact may be a consequence of the differences in the environments of each of the complexes.

Magnetic Susceptibility. The reciprocal molar magnetic susceptibility of powdered samples vs. temperature is plotted in Figure 4. The data were fitted to

$$\chi_M = C/(T - \Theta) + N\alpha \qquad (1)$$

where $N\alpha$ is the temperature-independent paramagnetism contribution. The best fit with parameters $C = 0.39$, $\Theta = 0$, and $N\alpha = 245 \times 10^{-6}$ emu/mol, is shown as a solid line in Figure 4. The Curie constant value $C = N_A g^2 \mu_B^2 S(S+1)/(3k)$ for $S = {}^1/_2$ leads to $g = 2.04$, which is much smaller than the g value, $g_{av}^{EPR} = 2.165$, determined from our EPR measurements. Fitting with

Table V. Geometrical Parameters and Optical Bands of D_{2d} Symmetry $CuCl_4^{2-}$ Complexes in Crystals

no.	compd	$\langle R \rangle$, Å	$\langle \beta \rangle$, deg	d–d bands, 10^3 cm^{-1}	CT bands, 10^3 cm^{-1}	ref
1	$(2tbpOH)_2CuCl_4$	2.225	55	6.3, 9.5	24.1	40
2	$CsCuCl_4$	2.230	64.6	4.8, 5.5, 7.9, 9.1	23.0, 24.8, 29.0	41, 42
3	$(NMe_4)_2CuCl_4$	2.230	64.7	6.0, 9.0	25.0, 36.0, 43.5	43, 44
4	$(TMBA)_2CuCl_4$	2.260	65	6.0, 9.0	22.7, 25.0, 29.4	45, 46
5	$[(C_2H_5)_3NH]_2CuCl_4$	2.240	67.5	8.0, 9.4		47, 48
6	$(Me_2NH_2)CuCl_5$	2.230	67.9	7.3, 10.7		49
7	$[(cinH_2)CuCl_4]_2 \cdot 3H_2O$	2.250	73	9.1, 11.1	22.5, 26.0	this paper
8	$(Me_2CHNH_3)_2CuCl_4$	2.266	78	10.0		50
9	$(MeNH_3)_2CuCl_4$	2.26	90	10.8, 13.3	24.0, 33.3, 38.5	43, 51
10	$(PhCH_2CH_2NMeH_2)_2CuCl_4$	2.265	90	16.1		52

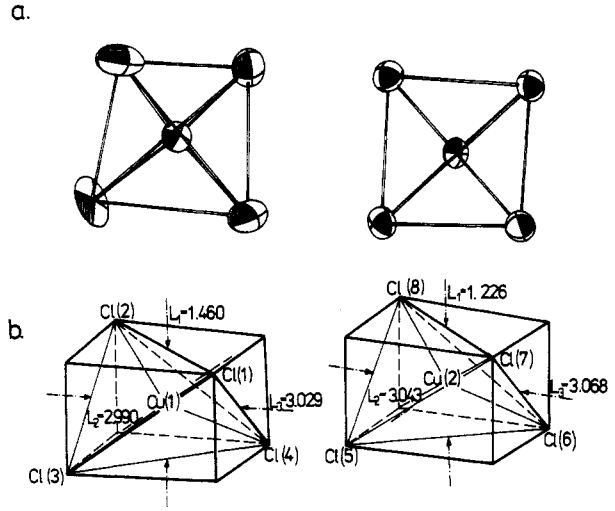

Figure 3. (a) ORTEP drawing of tetrahedral Cu complexes. (b) Relevant dimensions in the $CuCl_4^{2-}$ complexes.

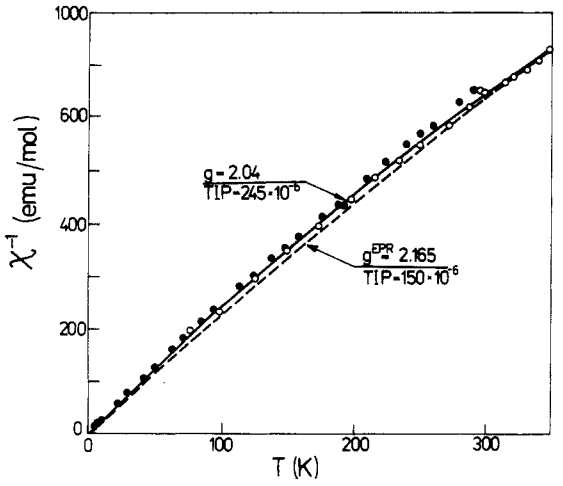

Figure 4. Powder molar susceptibility vs. temperature for two samples (open and solid circles). Two plots (solid line and dashed line) are the best fits as discussed in the text.

g_{av}^{EPR} leads to $N\alpha = 150 \times 10^{-6}$ emu/mol and is shown as a dashed line in Figure 4. Discrepancies with $g^{\chi} < g^{EPR}$ are commonly observed for copper(II) compounds[14-16] and are considered as a fairly good agreement by some authors,[16] although the difference $(g^{\chi} - g^{EPR})$ lies far from the experimental error region for both χ and EPR measurements. A reason for the inconsistency of g values from the two methods is due to a restricted validity of the simple Curie–Weiss equation (eq 1). To obtain a better fitting the higher order (in T) terms should be added as discussed by Van Vleck[17] and Arrott,[18] or the parameters in eq 1 should be recognized as temperature dependent. The Van Vleck paramagnetism contribution $N\alpha$ is slightly larger than that commonly assumed for six-coordinated Cu(II) complexes (60×10^{-6} emu/mol), but because of the lower orbital splitting in the tetrahedral crystal field the higher $N\alpha$-value can be expected. The Weiss constant, Θ, is equal to zero within experimental error, indicating a very small interaction between copper(II) ions.

EPR Results. The single-crystal EPR spectrum contains a single Lorentzian line or two poorly resolved lines depending on the crystal orientation. The perfect Lorentzian line shape observed along crystallographical axes and in the *ac* plane indicates a complete exchange averaging of the hyperfine splitting and local dipolar fields. The existence of a two-component spectrum in the *ab* and *bc* planes suggests that exchange coupling between copper(II) ions is of the order of the difference in Zeeman energy of magnetically nonequivalent Cu(II)-complexes in the crystal. Attempts to fit this spectrum with two independent Lorentzian lines were unsuccessful. It suggests that the exchange coupling is strong enough to produce the onset of a merging effect of the two EPR lines. In this case the shape $Y(B)$ of a two-component EPR spectrum, with lines at B_a and B_b, is described by eq 2.[19]

$$Y(B) = N\{[W_2 - 2(B - B_0)J](W_1^2 + W_2^2) - 4[(B - B_0)W_2 - (\Gamma_0 + 2J)W_1][(B - B_0)W_1 + (\Gamma_0 + J)W_2]\}(W_1^2 + W_2^2)^{-2} \quad (2)$$

where

$$W_1 = (B - B_a)(B - B_b) - (\Gamma_a + J)(\Gamma_b + J) + J^2$$

$$W_2 = (B - B_a)(\Gamma_b + J) + (B - B_b)(\Gamma_a + J)$$

Γ_j (j = a, b) is the half-width of the line and is related to the experimentally determined peak-to-peak line width: $\Gamma_j = 3^{1/2}(\Delta B_{pp}^{(j)}/2)$. N is a normalization factor and can be related to the total number of Cu(II) ions in a sample. B_0 and Γ_0 are averaged values of resonance fields and line widths of the two lines, respectively. The resonance fields and line width values are given in millitesla in eq 2, and J (mT) = 1069.75J (cm^{-1}) describes the exchange coupling with the Hamiltonian $\mathcal{H}_{ex} = -J\mathbf{S}_1 \cdot \mathbf{S}_2$.

A computer fitting of experimental spectra with eq 2 leads to the B_j and $\Delta B_{pp}^{(j)}$ values varying with crystal orientation and to the isotropic exchange integral $|J| = 0.0030$ (5) cm^{-1} at room temperature. The angular dependences of the resonance fields B_j and line width $\Delta B_{pp}^{(j)}$ are presented in Figure 5, where the points in the *ab* and *bc* planes were obtained by using eq 2. The data of these planes were then least-squares fitted to the g-factor anisotropy equation:

$$g^2(\theta) = \alpha + \beta \cos 2\theta + \gamma \sin 2\theta \quad (3)$$

The results indicate an axial $\mathbf{g}^2$-tensor symmetry. Thus the principal $\mathbf{g}^2$-tensor values can be directly calculated from two-plane data. $g_{\parallel}$ can be calculated as $g_{\parallel}^2 = g_a^2 + g_b^2 + g_c^2 - 2g_{\perp}^2$, where g_a, g_b, and g_c are g factors along crystallographic axes resulting from eq 3, and $g_{\perp}$ corresponds to the maximal resonance field, which is identical in the *ab* and *bc* planes. The resulting eigen-

(14) Estes, W. E.; Losee, D. B.; Hatfield, W. E. *J. Chem. Phys.* **1980**, *72*, 630–638.
(15) Marsh, W. E.; Patel, K. C.; Hatfield, W. E.; Hodgson, D. J. *Inorg. Chem.* **1983**, *22*, 511–515.
(16) Sikorav, S.; Bkouche-Waksman, I.; Kahn, O. *Inorg. Chem.* **1984**, *23*, 490–495.
(17) Van Vleck, J. H. *Physica (Amsterdam)* **1973**, *69*, 177–192.
(18) Arrott, A. S. *Phys. Rev. B: Condens. Matter* **1985**, *31*, 2851–2856.
(19) Hoffmann, S. K. *Chem. Phys. Lett.* **1983**, *98*, 329–332.

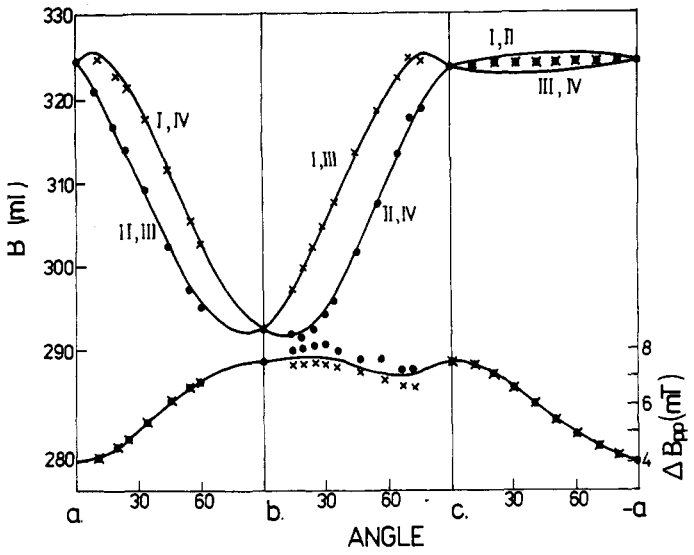

Figure 5. Angular dependence of the EPR resonance field B and line width ΔB_{pp} at 295 K. Points for B in the *ab* and *bc* planes were found from a computer simulation of the EPR spectrum, and solid lines are the resulting g^2-tensor angular dependence. I–IV denote the four magnetically nonequivalent complexes in the crystal unit cell.

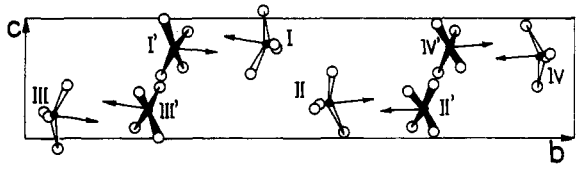

Figure 6. Two kinds (N and N') of crystallographically nonequivalent $CuCl_4^{2-}$ complexes in the *bc* plane. Arrows denote g^2-tensor z axes, which are mutually parallel in the pairs of complexes.

values are $g_\parallel = 2.292$ (4) and $g_\perp = 2.051$ (4). The z axis eigenvector components can be found from g-factor values as $l_z^2 = (g_a^2 - g_\perp^2)/d$, $m_z^2 = (g_b^2 - g_\perp^2)/d$, and $n_z^2 = (g_c^2 - g_\perp^2)/d$, where $d = (g_\parallel^2 - g_\perp^2)$, and $(l_z, m_z, n_z) = (0.1369, 0.9748, 0.1760)$.

The angular dependence of the resonance fields confirms an orthorhombic crystal symmetry, with, however, four magnetically nonequivalent but geometrically identical copper(II) complexes in the unit cell. The z axes of the complexes are close to the crystal b axis direction and form an angle of 13° with this axis. The z axis direction can be identified as the flattening axis of $CuCl_4^{2-}$ tetrahedron as is indicated by a comparison of direction cosines determined from EPR and from crystal data (see the description of the structure). The complexes in the unit cell differ in signs of the z axis direction cosines, which are I (+++), II (−+−), III (+−−), and IV (−−+). These axes are marked by arrows in Figure 6. The solid lines plotted for the magnetic field in Figure 5 result from principal g values and direction cosines for centers I–IV. The plot in the *ac* plane indicates a very small in-plane g-factor anisotropy resulting from near-perpendicular tetrahedron orientations in this plane. As a result the difference in Zeeman energy for magnetically nonequivalent I,II and III,IV complexes is smaller than the exchange coupling in the plane, and a single averaged line in EPR spectrum is observed.

EPR data indicate an existence of the four identical but differently oriented $CuCl_4^{2-}$ tetrahedrons in the unit cell. A relatively good resolution of the d–d bands in the optical spectrum (Figure 9) suggests also only one kind of $CuCl_4^{2-}$ complex in the crystal. It is surprising since two sets of magnetically nonequivalent $CuCl_4^{2-}$ complexes exist in the unit cell. The only explanation is that despite structural differences between the two kinds of complexes, the electronic structures are very similar and the local crystal field symmetry axes are close enough one to another to give unresolved lines in the EPR spectra. Two EPR arguments support this explanation: (i) The $J = 0.0030$ cm^{-1} $\simeq$ 3 mT determined by EPR seems to be slightly too low to produce a

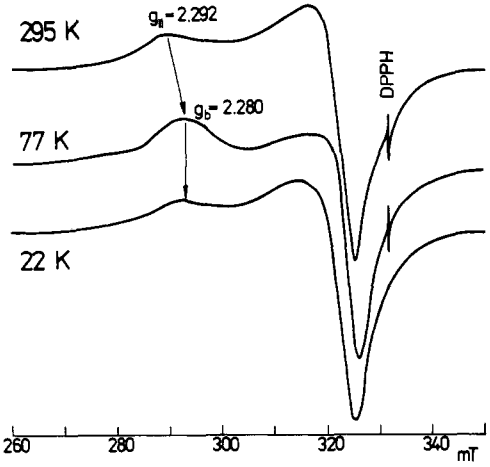

Figure 7. Temperature behavior of the powder EPR spectrum.

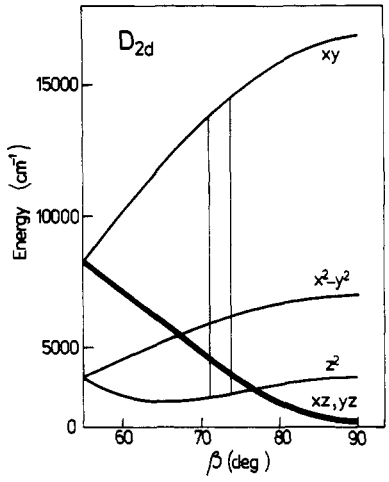

Figure 8. d-Orbital energies vs. flattening angle β. Two kinds of $CuCl_4^{2-}$ complexes are marked.

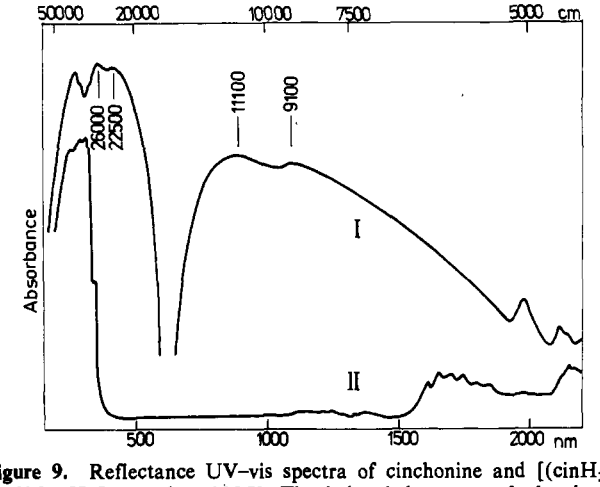

Figure 9. Reflectance UV–vis spectra of cinchonine and $[(cinH_2)CuCl_4]_2 \cdot 3H_2O$ crystals at 295 K. The d–d and charge-transfer bands are marked.

complete merging of the hfs lines as is evident from the perfect Lorentzian line. So, an additional exchange coupling between crystallographically nonequivalent Cu(II) sites must exist with $J' > J$. As a result the hfs lines as well as EPR lines from crystallographically nonequivalent Cu(II) complexes are merged completely. Thus a single Lorentzian line can be observed from crystallographically nonequivalent complexes that are very close in z-axis orientation like I and I′ or II and II′, as can be recognized in Figure 6. A similar situation has been found in $[M(en)_3]_2[Cu_2Cl_8]Cl_2 \cdot 2H_2O$ (M = Co, Rh, Ir) crystals where two superexchange pathways for interdimer exchange exist with differing

strengths of exchange coupling. (ii) In the light of a detailed complete merging effect discussion,[20] it is practically impossible to observe an axially symmetrical crystal EPR **g** tensor when a misalignment of the local crystal field axes exists in a crystal. So, the axiality of our **g** tensor suggests a coincidence of the local axes from crystallographically nonequivalent complexes, and the crystal **g** tensor can be considered as a molecular **g** tensor.

Thus, the closely packed nonidentical $CuCl_4^{2-}$ complexes in the unit cell (Figure 6) have the same angular dependence of the EPR spectrum. Also g factors, reflecting orbital splitting, are very similar as will be discussed below.

Temperature Effect in the EPR Spectrum. The temperature behavior of the EPR spectrum was observed on powdered samples and is presented in Figure 7. The line width is only slightly affected by temperature; thus, relaxation processes are overdominated by the exchange interaction. The parallel peak of the spectrum is shifted from the position $g_\parallel = 2.292$ at room temperature toward higher magnetic field when the temperature decreases, and at 77 K the peak is in the position $g_\parallel = 2.280$, which corresponds exactly to the g value along the b axis (see Figure 5, $B \parallel b$). This position is held down to 22 K.

This suggests a temperature averaging of the EPR lines resolved at 295 K in the *ab* and *ac* crystal planes. As a result the crystal EPR spectrum at low temperatures is observed with principal **g**-tensor axes along the crystallographic a, b, and c axes and principal values $g_a = 2.061$, $g_b = 2.280$, and $g_c = 2.053$. Thus the exchange coupling is temperature dependent in the crystal and the J value increases with lowering of temperature in a similar way as observed in some paramagnetic crystals.[21-24] It can be understood in terms of thermal lattice contraction resulting in a small shortening of intermolecular distances.[19,25,26]

Ligand Field Theory of d–d Bands. The $CuCl_4^{2-}$ complexes are deformed and have approximately a flattened tetrahedron D_{2d} symmetry. The flattening angle β (2β = Cl–Cu–Cl) is $\beta_T = 54.74°$ for an ideal tetrahedron and $\beta = 90°$ for a coplanar structure. A deformation of $CuCl_4^{2-}$ from a regular T_d or D_{4h} symmetry is an intrinsic property of the complex and is determined by a balance between the ligand field stabilization of the square-planar geometry and the destabilizing effect of ligand–ligand repulsions.[27,28] Ab initio calculations give an intrinsic value of $\beta = 60°$,[29] which is smaller than those observed in our crystal ($\beta = 74.1°$ and $\beta' = 71.1°$). Geometrical parameters of the D_{2d} deformation for our $CuCl_4^{2-}$ tetrahedrons are given in Table IV, where it can be seen that the average Cu–Cl distance is practically the same in both types of geometrically nonidentical complexes, while a small (3°) difference exists in averaged β-values.

The geometry and electronic structure of $CuCl_4^{2-}$ complexes were a subject of many theoretical studies as reviewed by Smith[30] and discussed by Solomon et al.[31] The theoretical approach to the problem of ligand field spectra is based on the electrostatic crystal field model[31-33] and/or the angular overlap model.[34]

The point-charge crystal field approach leads to underestimated d–d transition energies, although many experimentally observed effects can be explained in terms of this simple electrostatic theory.[33] Solomon et al.[31] used this approach for description of d–d transition energies in tetrachlorocuprates and blue copper proteins with CuN_2S_2 distorted tetrahedrons. They fitted experimental optical band positions with theoretical expressions using the radial crystal field parameters Ds and Dt and the β angle as fitting parameters (Ds and Dt are simply related to our a_2 and a_4 parameters, respectively). Good agreement has been found between calculated and experimental β values. The radial parameter values, however, seem to be unrealistic, and the Ds to Dt interrelation leads to metal–ligand distances lower than 1 Å. Thus, Solomon's approach can be used as a semiempirical method of crystal field theory, which reflects a crystal field geometry without keeping the relations of crystal field parameters to the electrostatic model.

A more realistic approach has been proposed by Smith[35] which took into account a destabilization of d orbitals by covalency of metal–ligand bonds described in terms of the angular overlap model. The electrostatic and covalency contributions can be treated separately, and the resultant d-orbital energies for D_{2d} distorted tetrahedron are

$$E_{xy} = (15\sin^4\beta)\delta^* + (5\sin^2 2\beta)\pi^* - {}^4/_7 a_2(3\cos^2\beta - 1) + (a_4/168)(-120\cos^2\beta + 35\cos 4\beta + 108)$$

$$E_{x^2-y^2} = (20\sin^2\beta)\pi^* - {}^4/_7 a_2(3\cos^2\beta - 1) + (a_4/42)(-30\cos^2\beta + 35\cos 2\beta + 3)$$

$$E_{xz,yz} = (7.5\sin^2 2\beta)\delta^* + 10(\cos^2 2\beta + \cos^2\beta)\pi^* + {}^2/_7 a_2(3\cos^2\beta - 1) + {}^2/_{21} a_4(35\cos^4\beta - 30\cos^2\beta + 3)$$

$$E_{z^2} = 20(\cos^2\beta - {}^1/_2\sin^2\beta)^2\delta^* + (15\sin^2 2\beta)\pi^* + {}^4/_7 a_2(3\cos^2\beta - 1) + {}^3/_{21} a_4(35\cos^4\beta - 30\cos^2\beta + 3) \quad (4)$$

where β is the flattening angle. The terms with a_2 and a_4 are the electrostatic energies, and $a_n = q\langle r^n\rangle/R^{n+1}$, where R is the Cu–Cl distance, q is the effective point charge of the ligands, and $\langle r^n\rangle$ is the mean n-power radii of the Cu(II) 3d orbital. For $\langle R\rangle = 2.25$ Å, $a_2 = 2400$ cm^{-1} and $a_4 = 514$ cm^{-1} were estimated. The terms with δ^* and π^* describe a destabilization of the d orbitals, with δ^* and π^* being proportional to the square of the appropriate diatomic overlap integrals. From Richardson's[36] radial 3d functions for copper(II) and Clementi's[37] chlorine 3p functions, $\delta^* = 1000$ cm^{-1} and $\pi^* = 300$ cm^{-1} can be estimated for a Cu–Cl distance of 2.25 Å.

A plot of E_{ij} energies vs. β for the above parameters is presented in Figure 8, where the positions for our complexes with β and β' are marked. The ground state is d_{xy}, as is confirmed by EPR data with $g_\parallel > g_\perp$. The difference in the orbital splitting between $CuCl_4^{2-}$ complexes with angles β and β' is very small; thus, a single optical absorption spectrum is observed for our crystal. Theoretically calculated d–d band positions averaged over the two kinds of complexes can be assigned as $(xy \leftrightarrow xz,yz) = 10\,400$ (±600) cm^{-1} and $(xy \leftrightarrow z^2) = 11\,150$ (±250) cm^{-1}. The $(xy \leftrightarrow x^2 - y^2)$ transition is symmetry forbidden. Experimentally observed d–d band positions (Figure 9) are at 9100 and 11 100 cm^{-1}. The agreement between theoretically predicted and observed d–d bands is fairly good in the light of the approximate D_{2d} symmetry of the complexes.

It is worthwhile to compare the above results with those obtained by using Solomon's approach. His method leads to the values $\beta = 71.8°$, $a_2 = 21D_s = 9240$ cm^{-1}, and $a_4 = 21D_4 = 7665$ cm^{-1}. Thus, the fitted β angle value is close to the average experimental value in the crystal (Table V). The fitted radial parameters, however, are strongly overestimated compared to our values calculated from electrostatic model.

(20) Hoffmann, S. K.; Szczepaniak, L. S. *J. Magn. Reson.* **1983**, *52*, 182–192.
(21) Kennedy, T. A.; Choh, S. H.; Seidel, G. *Phys. Rev. B: Solid State* **1970**, *2*, 3645–3651.
(22) Okuda, T.; Date, M. *J. Phys. Soc. Jpn.* **1970**, *28*, 308–311.
(23) Groenendijk, H. A.; Duyneveldt, A. J.; Willett, R. D. *Physica B+C (Amsterdam)* **1975**, *98B+C*, 53–57.
(24) Nakatsuka, S.; Osaki, K.; Uryu, N. *Inorg. Chem.* **1982**, *21*, 4332–4333.
(25) Zaspel, C. E.; Drumheller, J. E. *Phys. Rev. B: Condens. Matter* **1978**, *18*, 1771–1778.
(26) Hoffmann, S. K.; Hodgson, D. J.; Hatfield, W. E. *Inorg. Chem.* **1985**, *24*, 1194–1201.
(27) Felsenfeld, G. *Proc. R. Soc. London, A.* **1956**, *236*, 506–511.
(28) Elian, M.; Hoffmann, R. *Inorg. Chem.* **1975**, *14*, 1058–1065.
(29) Demuynck, J.; Veillard, A.; Wahgren, U. *J. Am. Chem. Soc.* **1973**, *95*, 5563–5569.
(30) Smith, D. W. *Coord. Chem. Rev.* **1976**, *21*, 93–158.
(31) Solomon, E. I.; Hare, J. W.; Dooley, D. M.; Dawson, J. K.; Stephew, P. J.; Gray, H. B. *J. Am. Chem. Soc.* **1980**, *102*, 168–178.
(32) Gerloch, M.; Slade, R. C. *Ligand Field Parameters*; Cambridge, England, 1973.
(33) Hoffmann, S. K.; Goslar, J. *J. Solid State Chem.* **1982**, *44*, 343–353.
(34) Jørgensen, C. K. *Modern Aspects of Ligand Field Theory*, North-Holland: Amsterdam, 1971; Chapter 10.
(35) Smith, D. W. *J. Chem. Soc. A* **1970**, 2900–2902.
(36) Richardson, J. W.; Nieupoort, W. C.; Powell, R. R.; Edgell, W. F. *J. Chem. Phys.* **1962**, *36*, 1057–1068.
(37) Clementi, E. *IBM J. Res. Dev., Suppl.* **1965**, *9*, 2–13.

In Table V are summarized geometrical and optical literature data for chlorocuprates(II). One can see that the deformation (β angle) of our $CuCl_4^{2-}$ complexes is one of the largest and the d–d transition is one of the highest in energy compared to those of the $CuCl_4^{2-}$ complexes in other crystals. The energy bands observed above 20 000 cm^{-1} in the optical spectrum of our crystal (Figure 9) can be assigned as charge-transfer absorptions commonly appearing in chlorocuprates(II) (see Table V).

MO Analysis of *g* Factors. It is well-known that it is impossible to predict theoretically the exact *g*-factor values either in terms of crystal field theory or even a simple Kivelson–Neimann MO approach.[38] According to Smith's critical review[39] the molecular orbital description should contain not only contributions from d-orbital mixing and orbital reduction effects but also contributions from charge-transfer, orbital overlap and ligand spin–orbit coupling. We will follow Smith's approach.

Taking the relevant antibonding MO's as

$$B_{2g} = b_1 d_{xy} - b_2 \phi_p(B_{2g})$$
$$B_{1g} = a_1 d_{x^2-y^2} - a_2 \phi_s(B_{1g}) - a_3 \phi_p(B_{1g}) \quad (5)$$
$$E_g = c_1 d_{xz,yz} - c_2 \phi_p(E_g)_E - c_3 \phi_p(E_g)_A$$

and the relevant bonding MO's as

$$B_{2g} = b_1' d_{xy} + b_2' \phi_p(B_{2g})$$
$$E_g = c_1' d_{xz,yz} + c_2' \phi_p(E_g)_E + c_3' \phi_p(E_g)_A \quad (6)$$

the *g* factors can be written as follows:

$$g_\parallel - 2.0023 = (8\lambda/E_1)(a_1 b_1 - a_3 b_2 \nu_L/2)(a_1 b_1 - a_3 b_2/2) + (8\lambda/E_{CT}^{(1)})(a_1 b_1' + a_3 b_2' \nu_L/2)(a_1 b_1' + a_3 b_2'/2) + \Sigma_1$$

$$g_\perp - 2.0023 = (2\lambda/E_2)(a_1 c_1 - 2^{-1/2} a_3 c_2 \nu_L)(a_1 c_1 - 2^{-1/2} a_3 c_2) + (2\lambda/E_{CT}^{(2)})(a_1 c_1' + 2^{-1/2} a_3 c_2' \nu_L)(a_1 c_1' - 2^{-1/2} a_3 c_2') + \Sigma_2 \quad (7)$$

where $E_1 = E_{x^2-y^2} - E_{xy}$, $E_2 = E_{xz,yz} - E_{xy}$, and $\lambda = 829$ cm^{-1} for Cu(II), and $\nu_L \simeq \lambda/\lambda_{Cl}$ ($\lambda_{Cl}^{3p} = 587$ cm^{-1}). The Σ_i are small corrections for δ overlap with ligand p orbitals, π-overlap orbitals, and ligand–ligand overlap and can be estimated as $\Sigma_1 = -0.055$ and $\Sigma_2 = -0.013$ in our crystal.

Taking $a_1 = b_1 = 1$, $b_1' = 0$, $\Sigma_1 = \Sigma_2 = 0$ and neglecting the second terms in parentheses of eq 7, one obtains the classical crystal field expressions. Taking $b_1' = 0$ and $\Sigma_1 = \Sigma_2 = 0$, and neglecting the second terms, one obtains the Kivelson–Neimann expressions.

All the a_i, b_i, and c_i parameters in eq 7 were calculated by Smith[39] for $CuCl_4^{2-}$ complexes. Using Smith's values and taking $E_{CT}^{(1)} = 22\,500$ cm^{-1} and $E_{CT}^{(2)} = 26\,000$ cm^{-1}, from the optical spectrum of our crystal (Figure 9), we have $g_\parallel = 2.3037$ and $g_\perp = 2.0556$, which agree well with the experimental values of 2.292 and 2.051, respectively.

Conclusions

In the compound presented in this paper copper(II) ions are four-coordinated in $CuCl_4^{2-}$ tetrahedrons with no direct coordination to the cinchonine molecules. Two kinds of crystallographically nonequivalent tetrahedrons are D_{2d} flattened as a result of interaction with cinchonine and water molecules in the crystal. The flattening is one of the largest among $CuCl_4^{2-}$ tetrahedrons in crystals. In spite of geometrical differences the electronic structures of the two kinds of Cu(II) complexes are quite similar, and the complexes are not distinguishable in EPR and UV–vis spectra. EPR parameters and absorption band positions can be assumed to be the molecular parameters of the individual $CuCl_4^{2-}$ complex in the crystal, which is confirmed by detailed MO analysis. Excellent agreement was found between MO calculations and experimentally determined EPR *g* factors and orbital energies for Cu(II) complexes.

Exchange coupling between Cu(II) ions is very weak; it is not detectable in the temperature dependence of magnetic susceptibility but is detectable in the range that can be observed by EPR spectroscopy as a broadening and shift of resonance lines. The exchange integral is equal to $|J| = 0.0030$ cm^{-1} at 298 K and increases at low temperatures.

Acknowledgment. This work was partially supported by the Polish Academy of Sciences, Grant R.P.II.10&13. The crystallographic section received financial support from the World Health Organization. The authors are greatly indebted to Professor M. Che, University Paris VI, France, for allowing measurements of reflectance spectra and to M. Chatry for recording the spectra. The authors wish to thank Professor P. Hagenmuller and Professor M. Pouchard, University Bordeaux I, France, for allowing measurements of magnetic susceptibility and Dr. J.-C. Grenier for help in performing the measurements. The authors are also grateful to the Regional Laboratory of Physico-Chemical Analyses and Structural Research, Kraków, Poland, for making the diffractometer available.

Registry No. $[(C_{19}H_{24}N_2O)CuCl_4]_2 \cdot 3H_2O$, 107494-92-8.

Supplementary Material Available: Tables of anisotropic thermal parameters for non-hydrogen atoms and hydrogen coordinates (4 pages); listings of observed and calculated structure factors (14 pages). Ordering information is given on any current masthead page.

(38) Kivelson, D.; Neimann, R. *J. Chem. Phys.* **1961**, *35*, 149–154.
(39) Smith, D. W. *J. Chem. Soc. A* **1970**, 3108–3120.
(40) Massabni, A. C.; Nascimento, O. R.; de Almeida Santos, P. H.; Francisco, R. H. P.; Lechat, J. R. *Inorg. Chim. Acta* **1983**, *72*, 127–130.
(41) Ferguson, J. *J. Chem. Phys.* **1964**, *40*, 3406–3412.
(42) McGinnety, J. A. *J. Am. Chem. Soc.* **1972**, *94*, 8406–8411.
(43) Willett, R. D.; Liles, O. L.; Michelson, C. *Inorg. Chem.* **1967**, *6*, 1885–1890.
(44) Clay, R.; Murray-Rust, J.; Murray-Rust, P. *Acta Crystallogr., Sect. B: Struct. Crystallogr. Cryst. Chem.* **1975**, *B31*, 289–295.
(45) Adams, D. M.; Lock, P. J. *J. Chem. Soc. A* **1967**, 620–624.
(46) Furlani, C.; Cervona, E.; Calzona, F.; Baldanza, B. *Theor. Chim. Acta* **1967**, *7*, 375–384.
(47) Lamotte-Brasseur, J.; Dupont, L.; Dideberg, O. *Acta Crystallogr., Sect. B: Struct. Crystallogr. Cryst. Chem.* **1973**, *B29*, 241–246.
(48) Lamotte-Brasseur, J. *Acta Crystallogr., Sect. A: Cryst. Phys., Diffr., Theor. Gen. Crystallogr.* **1974**, *A30*, 487–490.
(49) Willet, R. D.; Larsen, M. L. *Inorg. Chim. Acta* **1971**, *5*, 175–180.
(50) Anderson, D. N.; Willett, R. D. *Inorg. Chim. Acta* **1974**, *8*, 167–171.
(51) Furlani, C.; Sgamellotti, A.; Magrini, F.; Cardischi, D. *J. Mol. Spectrosc.* **1967**, *24*, 270–274.
(52) Harlow, R. L.; Wells, W. J.; Watt, G. W.; Simonsen, S. H. *Inorg. Chem.* **1974**, *13*, 2106–2110.